Journal of Geophysical Research: Oceans

RESEARCH ARTICLE
10.1002/2017JC013431

Coastal Upwelling Off Southwest Nova Scotia Simulated With a High-Resolution Baroclinic Ocean Model

Fatemeh Chegini[1,2], Youyu Lu[3], Anna Katavouta[1,4], and Harold Ritchie[5]

[1]Department of Oceanography, Dalhousie University, Halifax, Nova Scotia, Canada, [2]Leibniz Institute for Baltic Sea Research, Warnemünde, Germany, [3]Bedford Institute of Oceanography, Fisheries and Oceans Canada, Dartmouth, Nova Scotia, Canada, [4]Now at University of Liverpool, Liverpool, United Kingdom, [5]Environment and Climate Change Canada, Dartmouth, Nova Scotia, Canada

Key Points:
- A high-resolution baroclinic ocean model simulates coastal upwelling off Southwest Nova Scotia
- Tidal induced onshore near-bottom currents are significantly affected by Scotian Current
- Particle tracking reveals different behavior of particles entering the region from east and west

Correspondence to:
Y. Lu,
Youyu.Lu@dfo-mpo.gc.ca

Citation:
Chegini, F., Lu, Y., Katavouta, A., & Ritchie, H. (2018). Coastal upwelling off Southwest Nova Scotia simulated with a high-resolution baroclinic ocean model. *Journal of Geophysical Research: Oceans*, *123*, 2318–2331. https://doi.org/10.1002/2017JC013431

Received 4 SEP 2017
Accepted 10 FEB 2018
Accepted article online 15 MAR 2018
Published online 2 APR 2018

Abstract A high-resolution baroclinic coastal ocean model is applied to study seasonal circulation and upwelling off South West Nova Scotia (SWNS) based on 1 year simulations for 2010. The model reasonably reproduces tidal currents, seasonal hydrography, and circulation from multiyear observations, in consistence with the observed strong seasonal variations of these properties in the study area. The main physical processes affecting circulation are analyzed using numerical experiments, with focus on the effect of tidal and density induced currents on topographic upwelling. It is confirmed that the shoreward near-bottom currents and associated upwelling are tidally induced and persistent throughout the year. It is revealed that these currents have seasonal variability, with cross-isobath component being strong in summer throughout a large area, but weaker and confined to deeper regions in winter. The seasonal variability of Scotian Current is the dominant forcing affecting the variability of onshore bottom currents. Lagrangian particle tracking identifies two major pathways of source waters arriving at the SWNS upwelling region. A large proportion of particles come from the east with the Scotian Current, mostly from the surface layer; and a small portion of water parcels come from a mean depth exceeding 100 m from the Gulf of Maine and Northeast Channel.

1. Introduction

Global and regional operational ocean forecast systems have been widely developed in recent decades with spatial resolutions of up to a few kilometers. However, to better resolve local dynamics for practical applications such as fisheries and marine search and rescue, higher resolution models are often necessary. As computational cost increases with increasing resolution, downscaling from large to regional scale can be adopted. The present study is part of a larger effort to develop relocatable high-resolution ocean forecasting models by downscaling from global and regional systems. The developed model covers the coastal waters off Southwest Nova Scotia (SWNS) and is applied to study the seasonal variability of circulation and upwelling in the region.

The coastal waters off SWNS play a significant role in the oceanography of the region. Lying between the Scotian Shelf (SS) and the Gulf of Maine (GoM) (Figure 1), this area is a pathway for transport of freshwater from the Gulf of St. Lawrence to GoM (Sutcliffe et al., 1976) and the seasonal changes in this transport are influential on the water mass budget of GoM (Smith, 1983). Due to strong tidal currents over shallow water depth, this area makes a significant contribution to the total dissipation of tidal energy in the GoM/SS region (Chen et al., 2011). On a regional scale, the coastal waters off SWNS are one of the most productive areas on the eastern coast of North America (Smith, 1983). The high biological activity related to upwelling of nutrient-rich deep waters is crucial for major fisheries of various species in this area.

Many studies have contributed to the understanding of the dynamics of this area, either as part of a larger scale study or as a locally focused regional study. On a regional scale, Smith (1983, 1989) used field data and diagnostic models to analyze the mean, seasonal, and interannual variability of circulation and its dynamical balance. On a larger scale, Hannah et al. (2001) applied a prognostic model to obtain the 3-D seasonal circulation and hydrography on the western and central Scotian Shelf and used the

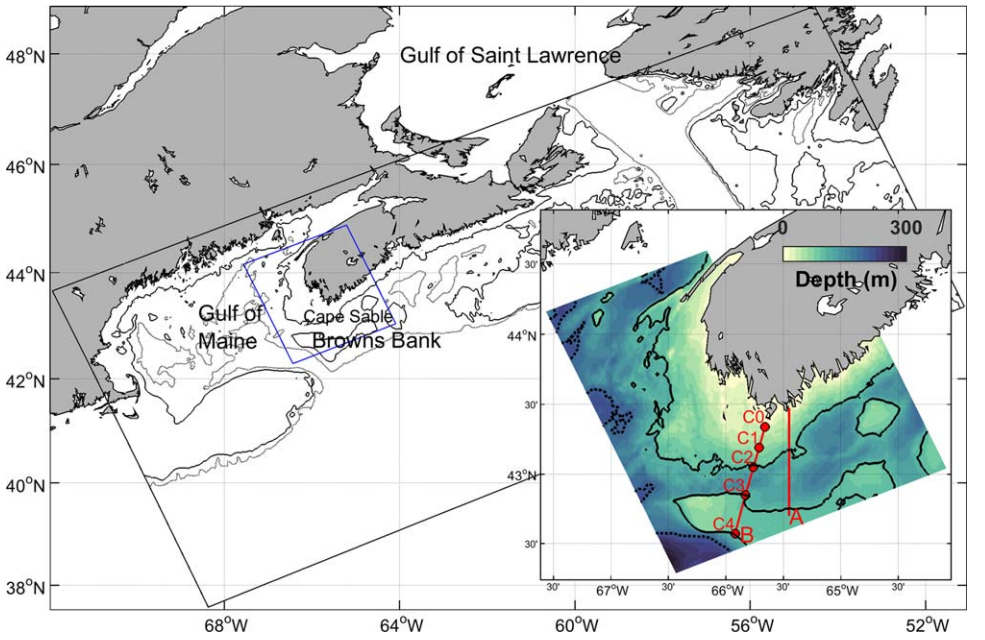

Figure 1. Southwest Nova Scotia and adjacent regions. Black box shows the boundaries of the regional GoMSS model domain. The high-resolution SWNS model domain is enclosed by the blue line. Inset plot: high-resolution model bathymetry. Lines A and B indicate sections used for evaluating the model results and analyzing physical processes, respectively. Solid circles show the locations of C0–C4 mooring stations. In both plots, solid black and dashed black contours depict 100 and 200 m isobaths, respectively.

results to describe the origin of the spatial structure of the currents. In a recent study, Katavouta et al. (2016) and Katavouta and Thompson (2016) developed a 3-D circulation model for the GoM/SS region with a horizontal resolution of approximately 2.5 km. The model realistically predicts the circulation and hydrographic variation of this region. Previous researchers have also focused on studying the tidal currents and rectification which contribute to coastal upwelling off SWNS (Greenberg, 1979; Tee et al., 1988, 1993).

Coastal waters off SWNS are characterized by cold and nutrient-rich surface waters during summer. Previous studies have shown that local upwelling combined with tidal mixing contribute to the high-levels of productivity in this region (Fournier et al., 1984; Tee et al., 1993). Based on a barotropic tidal model, Tee et al. (1993) revealed that tidal rectification generates cross-isobath onshore currents that bring water parcels from deeper regions to shallower areas and the water parcels are then vertically transported to the surface by strong tidal mixing. These shoreward bottom currents are evident from observations with seabed drifters (Lauzier, 1967) and moorings (Lively, 1985). Although the mechanism for creating onshore currents has been identified, the effects of baroclinicity on these currents have not been addressed. Furthermore, the origin of the water parcels entering the upwelling area is not clear. In this study, these aspects are studied using a regional baroclinic model and particle tracking.

The SWNS model developed in this study is downscaled from a larger model covering the GoM/SS region described by Katavouta et al. (2016). Afer evaluating the simulated tidal and seasonal currents and hydrography of the region, numerical experiments are carried out to identify the role of physical processes on the circulation. The main focus is to quantify the contribution of processes to cross-isobath currents, which are postulated to result in upwelling of deep waters. Finally, the origin and transport pathway of upwelled water are studied by applying particle tracking.

The paper is structured as follows. The coastal model and design of the experiments are described in section 2. In section 3, the model results are evaluated against observations and used to describe seasonal changes in currents and hydrography. The physical processes that contribute to seasonal circulation off SWNS are studied in section 4, focusing on the variation of the cross-isobath onshore currents. Section 5 presents the results of particle tracking. A summary is provided in section 6.

2. Model and Simulation Experiments

The model developed in this study is based on the ocean component of version 3.6 of the Nucleus for European Modeling of the Ocean (NEMO) (Madec, 2008). The model domain includes an area of approximately 200 × 250 km shown in Figure 1. The model uses initial and boundary conditions from the GoMSS model of Katavouta et al. (2016).

A multisource bathymetry data set that includes high-resolution in situ observations is used to create the bathymetry for the model. This data set was compiled by H. Varma (personal communication, 2013) at the Bedford Institute of Oceanography (BIO), Fisheries and Oceans Canada. The BIO data are processed to be referred to the mean water level and then interpolated to model grids. Gaps in the BIO data are filled with the 1 arc min gridded global relief data set of ETOPO1 (Amante & Eakins, 2009) using the statistical (optimal) interpolation method (Daley, 1993). Details of the processing of bathymetry data will be reported elsewhere.

The average horizontal resolution of the SWNS coastal model is approximately 700 m and 40 z-levels are used in the vertical. The spacing of vertical levels varies from 0.5 m at the surface to 12 m at the deepest level. The maximum water depth is 305 m. Bottom partial steps are employed for a better representation of varying bathymetry with the minimum depth set to 5 m. A variable volume level scheme is used to allow the stretching of the thickness of vertical levels according to changes of sea surface height (Levier et al., 2007). The bottom friction is parameterized using a quadratic formulation related to the velocity of the bottom level. The bottom drag coefficient (C_d) is calculated from a logarithmic boundary layer equation given by Chen et al. (2001) with bottom roughness set to 0.003 m and maximum C_d being 0.002. The time-splitting scheme is applied with the barotropic and baroclinic time steps set to 3 and 60 s, respectively. The vectorial form for momentum advection is chosen, allowing conservation of both energy and enstrophy. The tracer advection uses the total variance diminishing scheme.

The parameterization of vertical subgrid-scale mixing is based on the k-ε configuration of the generic length scale turbulence closure scheme (Umlauf & Burchard, 2003). The background values for vertical eddy viscosity and diffusivity are 10^{-5} and 10^{-6} m^2 s^{-1}, respectively. The parameterization of lateral mixing is based on down-gradient Laplacian diffusion with horizontal diffusion and viscosity coefficients determined by the Smagorinsky scheme (Smagorinsky, 1963). The lateral mixing operates along geopotential surfaces for momentum and isopycnal surfaces for tracers. The background lateral eddy viscosity and diffusivity are set to 1 m^2 s^{-1}.

The prescribed initial conditions include temperature and salinity. The lateral open boundary conditions have two different frequencies, i.e., daily and hourly. The baroclinic currents (total flow minus the depth-averaged value) and tracers are obtained from daily-averaged values of GoMSS. Sea surface height and depth-averaged currents are obtained from hourly snapshot of GoMSS output. Five tidal constituents (M2, S2, N2, K1, and O1) are included. The applied open boundary conditions differ for each variable. A flow relaxation scheme (Engedahl, 1995) is used for the tracers and baroclinic velocities with a relaxation width of 10 grid lengths inside the lateral boundary. The radiation scheme of Flather (1994) is applied for the barotropic current normal to the lateral open boundary, using the depth-integrated velocity and sea surface height from GoMSS.

The atmospheric forcing data are taken from the Canadian Meteorological Centre's Global Deterministic Prediction System Reforecasts (CGRF), which has a resolution of approximately 30 km (Smith et al., 2014). The included variables are hourly wind fields (at 10 m), air temperature, and humidity (at 2 m), precipitation and short and longwave radiation. The heat fluxes are computed using the CORE bulk formulae (Large & Yeager, 2004). There are no major rivers along the coastline of the model domain. The runoff from local small rivers is not included, since its influence on salinity variation in the study region is small compared to the lateral freshwater transport carried by the Scotian Current.

The model is run with three experiments, starting from 1 January 2010 and lasting the whole year. The control run, named Full, includes the complete set of forcing of momentum and heat fluxes at the surface and lateral open boundary. The second run, named NoTide, is similar to Full with the exception of excluding tidal forcing at the lateral boundary. Lastly, a barotropic tidal run, named BrtTide, sets temperature and salinity to be constant and is only forced with barotropic tides from the lateral open boundary. This run

does not include atmospheric forcing. The spin-up time for the model simulations is in the order of 3–5 days according to the time series of the domain-averaged total kinetic energy (figures not shown). The rapid spin-up is due to the simulations starting in January when the water column is well mixed; hence, the spin-up is primarily for the barotropic component.

In addition to the ocean model, a particle tracking model is used to track and analyze the trajectory of particles released in the model domain. For this purpose, the Ariane offline computational tool is applied (Blanke & Raynaud, 1997). Ariane uses the 3-D velocity field of an ocean model to calculate streamlines and main pathways of particles but does not include random-walk. Ariane can perform both forward and backward integration to track the final and initial positions of particles. In this study, backward tracking is used to determine the origin of water mass in the upwelling region off SWNS.

3. Model Evaluation

In this section, the model performance is evaluated by comparing model results with various observations including current-meter, tidal, and hydrography data. Furthermore, the model results are used to describe the tidal currents and seasonal variability of circulation and hydrography off SWNS. The observational data are obtained from the BIO archive (Ocean Data Inventory, http://www.bio.gc.ca/science/data-donnees/base/data-donnees/odi-eng.php). Current-meter and hydrography data are from four mooring stations (C0–C4 shown in Figure 1) deployed from 1979 to 1983 in the SWNS region (Lively, 1985). The tidal ellipse parameters are derived from data with record lengths of more than 30 days.

The robustness of characterizing the seasonal variation off SWNS using 1 year model simulation is supported by observations. Smith (1989) analyzed observed time series at mooring site C2 over 6.5 years (1978–1985) and at C1 over 4 years (1979–1985). The analysis was carried out for three depths, i.e., near the surface (15 m), middepth, and at 10 m above the bottom. The analysis showed strong seasonal variations in temperature, salinity, and currents at both sites. Near the bottom, strong onshore current occurred in late summer (July and August) at both stations in all years. Near the surface at C2, and at middepth at C2 and at C1, the along-shore current was strong and directed westward in winter, but weak in summer. At C1, low values of near surface temperature, ranging 6–8°C, were present in late summer in all years. Combining the data analyzed by Smith (1989), hydrographic data from 1979, and Lagrangian drift measurements from 1983 to 1985, Tee et al. (1993) revealed that off SWNS the topographic upwelling associated with cross-isobath currents occurred yearly.

3.1. Tidal Currents

Tidal currents and elevations are relatively well known in the study area (Greenberg, 1979; Ohashi et al., 2011) and are well simulated by the GoMSS model that provides the tidal forcing for the SWNS model. It is known that the near resonant lunar semidiurnal tide (M2) is responsible for the large tidal range in the region (Tee et al., 1993) and is therefore the main focus of this study. Figure 2 shows the ellipses of depth-averaged M2 tidal currents calculated from the BrtTide run. The simulated tidal currents have considerable spatial variation in the study domain, with strong tidal currents in the shallower region near Cape Sable (up to 1.5 m s^{-1}) and over Browns Bank and weaker currents in the eastern part of the domain.

Figure 3 shows the comparison of M2 tidal ellipses from the BrtTide run and observations at three representative depths (upper, middle, lower) at four mooring stations (C1–C4). Note that station C1 is located in a shallower region with a water depth of approximately 50 m, while the other three stations are in deeper regions with depth of about 110 m. Both model and observation results show relatively weak vertical variability of tidal currents. The small vector differences between observed and simulated ellipses demonstrate the satisfactory performance of the model in predicting tidal currents, even if running in barotropic mode. This is consistent with the weak seasonal variation of tidal currents in our study area according to the fully baroclinic simulation of GoMSS (Figure 5, Katavouta et al., 2016). This also suggests the weaker contribution of internal tides (ITs) to the total tidal currents. Note that the use of daily-averaged baroclinic velocity from GoMSS at the lateral open boundaries prevents the remotely generated ITs propagating into the model domain. The Full run should include locally generated ITs, but their contribution to the total tidal currents is small according to the weak vertical variation of tidal ellipses.

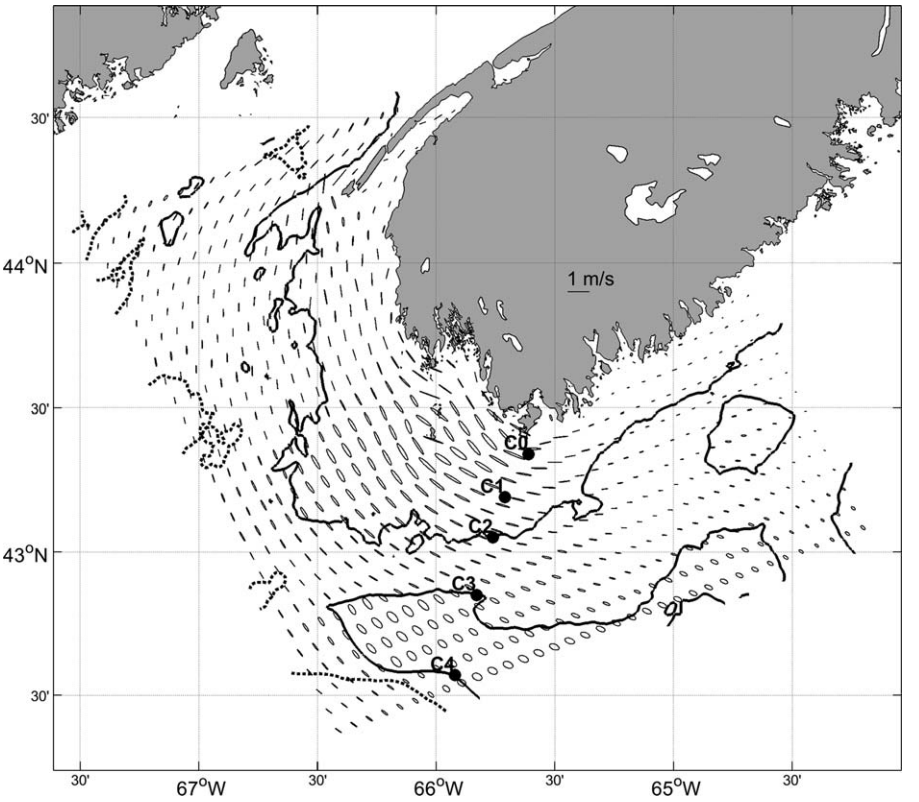

Figure 2. Depth-averaged M2 tidal ellipses from BrtTide simulation. Solid circles show the locations of C0–C4 mooring stations. Ellipses are shown for every 10th grid point. Solid black and dashed black contours depict 100 and 200 m isobaths, respectively.

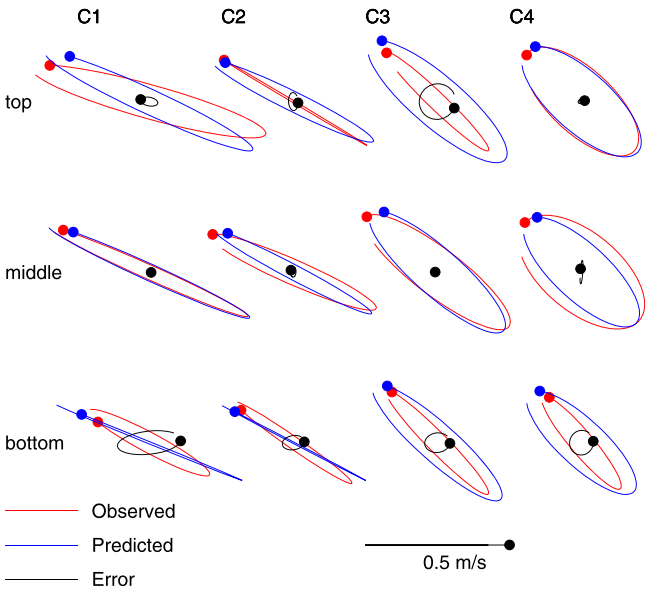

Figure 3. Comparison of M2 tidal ellipses from observations (in red) and BrtTide model simulation (in blue) at C1–C4 mooring stations for three depths. The dot denotes the starting time (the same for each ellipse). The last 1/12 of the tidal cycle is not plotted, allowing one to deduce the sense of rotation. The vector error is shown in black.

The calculated depth-averaged tidal residual currents induced by M2 tides (not shown) are in agreement with the previous study of Tee et al. (1993). The main features of these currents include the anticyclonic tidally rectified gyre on Browns Bank, the high westward tidal residual currents (exceeding 0.15 m s^{-1}) in shallow areas near Cape Sable, and the shoreward current at section A (Figure 1) which is present in the nearshore zone within the 110 m isobath.

3.2. Seasonal Circulation

The seasonal velocity fields averaged for the top 100 m depth in winter (January–March) and summer (July–September), calculated from the Full run, are shown in the upper plots of Figure 4. The general features of the circulation include the westward Scotian Current entering from the eastern boundary along the coast, the outflow into the Bay of Fundy at the northern boundary and the persistent anticyclonic gyre on Browns Bank (position of Bank denoted in Figure 1) due to tidal rectification (Tee et al., 1993). The distribution and seasonal variation of the circulation are consistent with previous studies (Hannah et al., 2001; Katavouta et al., 2016; Smith, 1983). The seasonal variation of modeled transport off SWNS is in very good agreement with observations. The model predicts 1.3 Sv annual mean volumetric transport past Cape Sable, with 3.1 Sv in winter (January–February) and 0.08 Sv in summer (July–August). The transport is calculated across section B (Figure 1) extending from the coast to about the 150 m isobath. Based

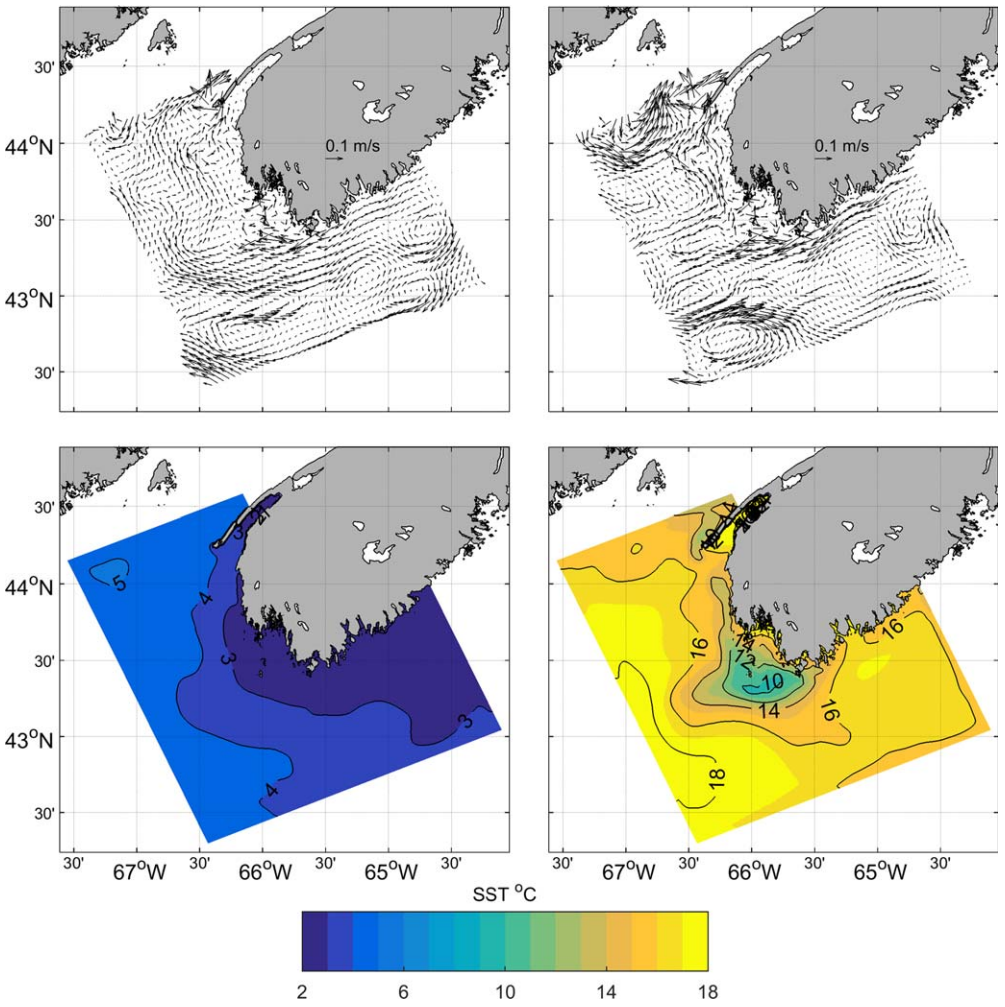

Figure 4. Full simulation results: (upper row) seasonal-mean depth-averaged velocities for the top 100 m depth and (lower row) sea surface temperature, for (left column) winter and (right column) summer.

on current-meter observations from C0 to C4 moorings along the same section, Hannah et al. (2001) estimated that the annual mean, winter, and summer volume transport past Cape Sable are 1.4, 3.2, and 0.03 Sv, respectively. The seasonal variation in transport off SWNS is related to that of the Scotian Current originating from the Gulf of Saint Lawrence and having a minimum in summer (Dever et al., 2016). The effect of this variability on upwelling off SWNS is discussed in the next section.

Figure 5 compares the along-shore and cross-shore seasonal-mean currents from the Full simulations and mooring observations along section B. Overall, the predicted currents are in good agreement with observations although vertical and horizontal offsets are detected. In winter, the modeled along-shore westward current extends from the coast to near C3 throughout the water column. In summer, the westward current is limited from the coast to C1 and a weak subsurface westward flow occurs at C2, consistent with observations. At C2, a near-bottom eastward current is detected in observations and model results, related to deep inflows in the Northeast Channel (Hannah et al., 2001). The anticyclonic gyre on Browns Bank with eastward current on its northern flank (C3) and westward current on its southern flank (C4) persist throughout the year, with the predicted vertical structure in agreement with observed profiles. The upper layer current at C0–C4 shows significant difference between summer and winter. This seasonal variation is related to that of the surface Ekman transport direction, which has a westward component in winter and an eastward component in summer. Regarding the cross-shore velocity, the model simulates a stronger near-bottom onshore velocity from station C1 to C2 in summer than in winter, although it under predicts this current at C1 in summer.

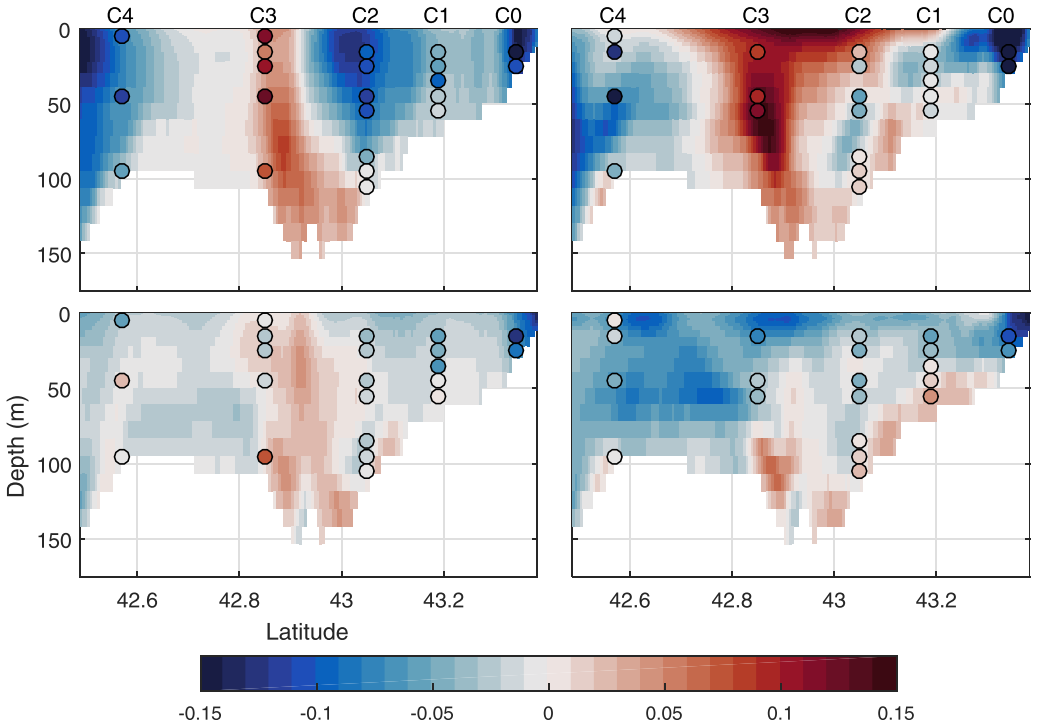

Figure 5. Full simulation results: (upper row) seasonal-mean along-shore and (lower row) cross-shore currents along section B (color shading outside circles), for (left column) winter and (right column) summer. Corresponding mooring observations (C0–C4) are shown by color shading inside circles. Color axis denotes velocity in m s^{-1}. Positive values indicate eastward flow for along-shore component and northward for cross-shore component.

3.3. Seasonal Hydrography

The seasonal changes in sea surface temperature and vertical hydrographic structure along section B are illustrated in Figures 4 and 6, respectively. In winter, the water is weakly stratified, while in summer, the stratification is stronger except for the well mixed upwelling region, consistent with observations. In summer, the model simulates the uplifting of thermocline and pycnocline near station C1, although it overestimates the temperature in the upper layer. Regarding salinity, the model is able to present the throughflow of fresher water at C1 and C2 in winter and the inflow of saline water at depth at C2 and C3 in summer. Previous studies (Hannah et al., 2001; Smith, 1989) have shown that this saline water originates from Georges Basin and is related to deep inflows in the Northeast Channel. The effect of this inflow on upwelling is discussed further in section 5.

4. Physical Processes

In order to separate the role of different processes that contribute to circulation off SWNS, results from the three experiments described in section 2 are analyzed. The role of all processes excluding tidal forcing is estimated from NoTide. These processes are forced by winds, heat, and freshwater fluxes at the sea surface in the model domain and the remote forcing outside the domain (included in the lateral open boundary condition). The contribution of tidal forcing is estimated by subtracting NoTide from Full results, hereafter named FullTide. This contribution consists of tidal residual and tidal mixing. Effect of stratification on tidal residual is also included in FullTide. The barotropic tidal residual is estimated from BrtTide. The analyses are carried out for along-shore and cross-shore currents for winter (Figure 7) and summer (Figure 8) along section A (shown in Figure 1). According to model results, cross-shore currents which contribute to coastal upwelling off SWNS are strongest at this section, in agreement with previous studies (Tee et al., 1993).

4.1. Along-Shore Current

In winter (Figure 7), the Full solution shows that strong westward flow is present over most of the section and extends from the surface up to 75–100 m depths. The NoTide solution shows a similar pattern,

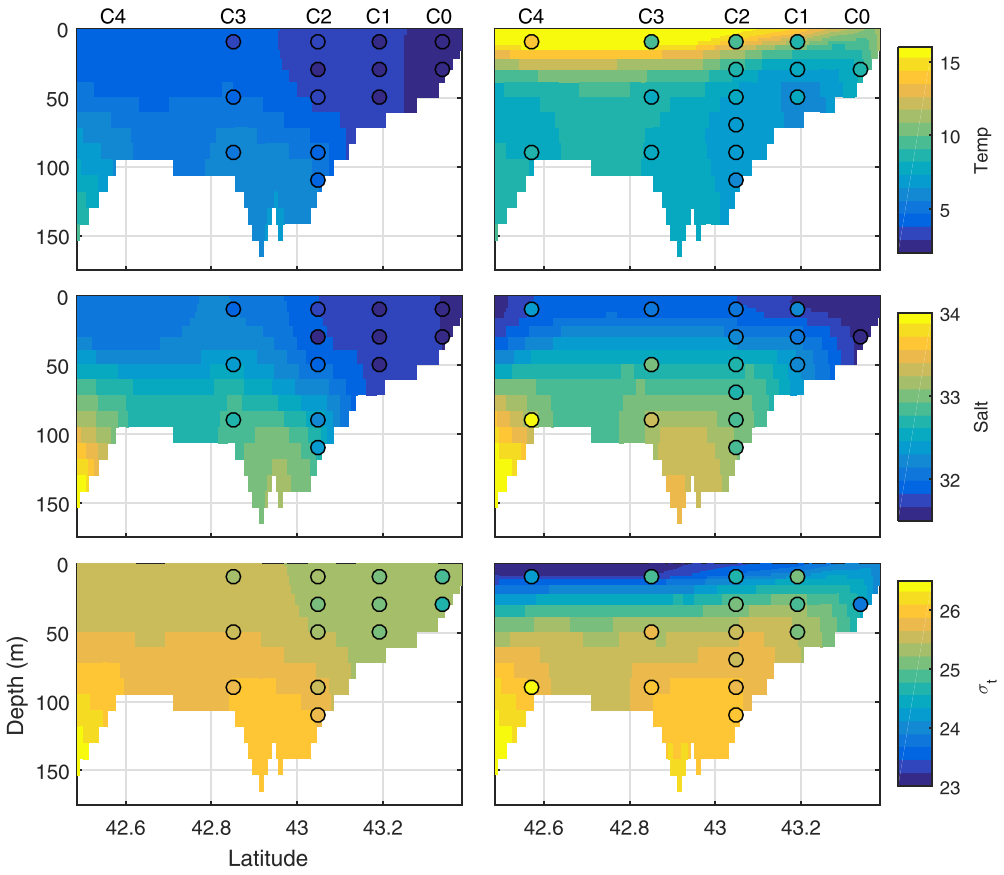

Figure 6. Full simulation results: (top row) seasonal-mean temperature (°C), (middle row) salinity (psu) and (bottom row) σ_t (kg m^{-3}) along section B (color shading outside circles) for (left column) winter and (right column) summer. Corresponding mooring observations (C0–C4) are shown by color shading inside circles.

confirming that overall, the westward Scotian Current is not generated by tidal forcing. Near the coast, the westward flow detected in the Full simulation is weaker in FullTide and stronger in BrtTide. The difference between FullTide and BrtTide indicates the contribution of tidal mixing. Further offshore, it is clear that tidal residual currents tend to oppose the westward Scotian Current.

In summer (Figure 8), the Full run shows that the westward current is restricted to the top 50 m layer and confined to the nearshore area. Again, NoTide shows a structure of along-shore current similar to the Full run. Further offshore, between 43°N and 43.2°N, a weaker westward subsurface current is present in NoTide but not in Full run. Tidal effects partly contribute to the formation of westward nearshore current, as seen by the results of FullTide and BrtTide. On the other hand, the Full run shows the presence of an eastward offshore current, which is strong in the upper 50 m layer. This eastward current has both a nontidal and a tidal component. The nontidal component is due to the eastward component of Ekman transport in summer. The tidal residual is enhanced by tidal mixing. The comparison between FullTide in summer and winter suggests that tidal mixing has the most significant contribution to nearshore westward flow in summer.

4.2. Cross-Shore Current

Previous studies have shown that upwelling off SWNS is initiated by tidal rectification, referred to as topographic upwelling (Tee, 1994; Tee et al., 1993). In this process, the tidal residual current flowing over large variations of bottom topography has a cross-isobath onshore component which advects water parcels from deeper to shallower areas. When the longshore coastal current is strong, the cross-isobath transported water parcel is carried away and is not transferred to upper layers. However, if the water parcels are advected into the strong tidal mixing area, they can be efficiently mixed into upper layers. Therefore, tidal rectification combined with tidal mixing are the mechanisms that describe coastal upwelling off SWNS.

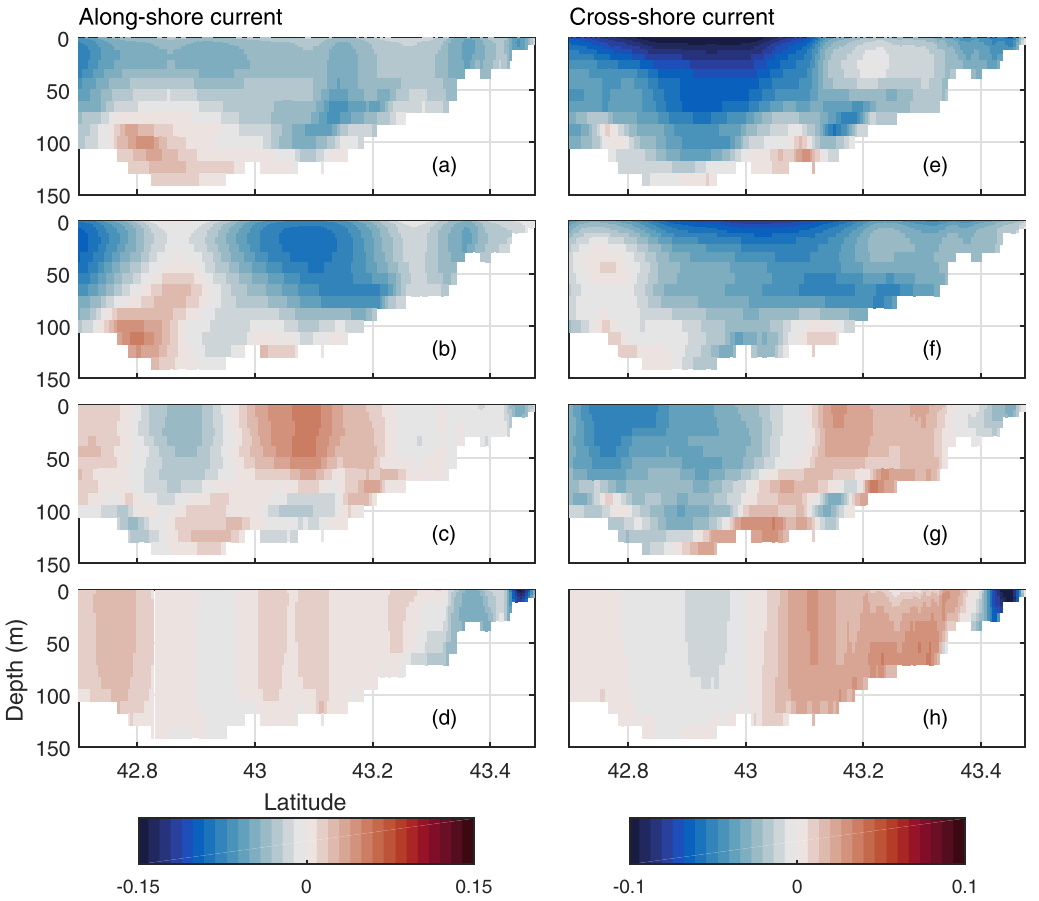

Figure 7. (left) Along-shore and (right) cross-shore currents along section A in winter, from (a, e) Full, (b, f) NoTide, (c, g) FullTide, and (d, h) BrtTide runs. Color axis denotes velocity in m s^{-1}. Positive values indicate eastward flow for along-shore component and northward for cross-shore component.

In winter (Figure 7), the Full run shows that the direction of cross-shore current along section A is mainly offshore and a weak bottom onshore current only appears in a small area of the section. NoTide shows a pattern similar to the Full run. The FullTide and BrtTide runs both depict a strong onshore cross-isobath current exceeding 4 cm s^{-1} in the tidal mixing region. This current is fairly uniform in the entire water column and slightly stronger near the bottom. Comparison of the Full, NoTide, and FullTide results demonstrates that in winter, the tidally induced onshore current is opposed by a strong offshore component of the Scotian Current. Therefore, in winter, onshore current is detected only in a very small area of deeper regions off SWNS.

In summer (Figure 8), the Full run shows a strong subsurface onshore current in the tidal mixing region between 43°N and 43.2°N, exceeding 4 cm s^{-1}. In the nearshore region, a strong offshore directed current is depicted. The NoTide run shows a similar pattern in the nearshore region but does not reproduce the onshore current between 43°N and 43.2°N. Instead, the onshore current is present in both FullTide and BrtTide runs, with the solution of FullTide being closer to the Full run. The comparison confirms that the onshore current is initiated by tidal residue and modified by tidal mixing.

Overall, model simulations show that the onshore currents are much stronger in summer compared to winter. This seasonal variation is also detected from observed current at C1 and C2 mooring stations (Figure 5). The difference in stratification condition between winter and summer is one contributing factor. Lee and Beardsley (1999) showed that in the Yellow Sea, the tidally induced cross-shore current in the bottom mixed layer under stratified condition is stronger than in homogenous water. Chen et al. (1995) showed that tidal rectification can be strengthened by nonlinear interactions between barotropic and internal tides, as well as between internal tidal currents themselves. Another contributing factor is the seasonal variation of the Scotian Current. The offshore directed component of the Scotian Current opposes the tidally induced onshore

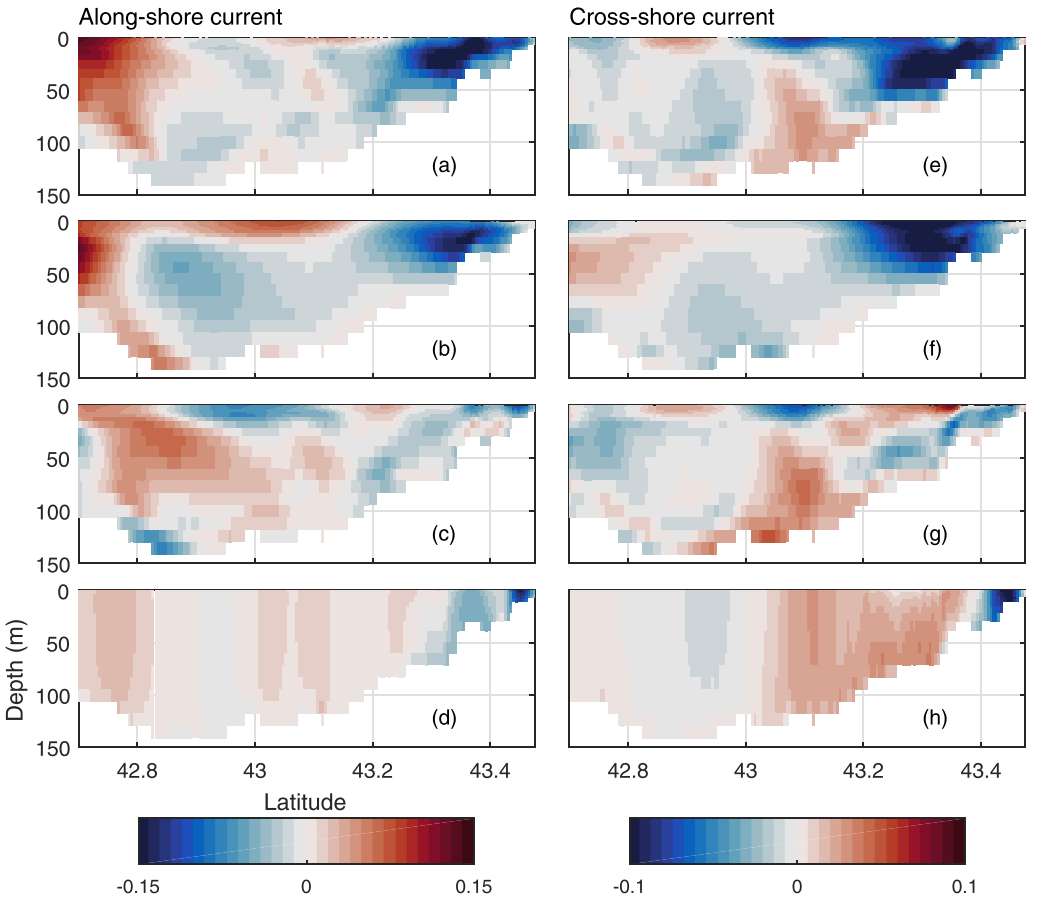

Figure 8. Same as Figure 7 but for the summer season.

currents. In winter, the Scotian Current is stronger and covers a large area. Therefore, the small amount of water advected shoreward is carried away by the increased along-shore NS current and blocked from entering the strong tidal mixing region, hence interrupting the upwelling process until late spring. In summer, with the decrease of the Scotian Current and its confinement to the nearshore region, the tidally induced onshore currents are not blocked. Therefore, the water advected onshore enters the strong tidal mixing area and is vertically mixed to the surface.

5. Particle Tracking

In this section, Lagrangian particle tracking is applied to analyze the pathway of source waters arriving at the upwelling region off SWNS. First, the particles are passively advected by hourly snapshots of three-dimensional (3-D) velocity fields obtained from the Full run. To determine the source waters, particles are released in the upwelling region and are advected backward in time. A similar approach has been used in previous studies on analysis of upwelling source waters using particle tracking (Mason et al., 2012; Rivas & Samelson, 2011). To avoid confusion of terminologies, in the following discussion, physical particle origin and final positions correspond to particle locations at the end and beginning of the backward tracking, respectively.

The physical final positions of 1,506 particles for backward tracking are specified every 5 days for one month in winter (from mid-February to mid-March) and summer (August), resulting in a total of 9,036 particle paths for each season. The final positions are distributed evenly from 10 to 50 m depth with a horizontal and vertical spacing of 1 km and 2 m, respectively. No particles are distributed in the top 10 m water column, where strong mixing due to wind forcing may exist. The effects of mixing and diffusion on trajectories

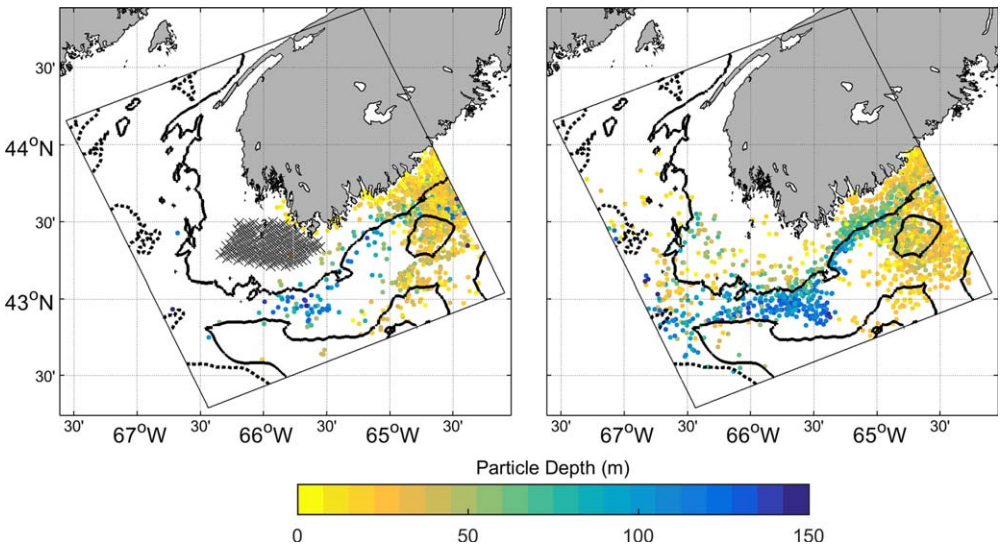

Figure 9. Seasonal original positions of particles 30 days before arriving at the final positions in upwelling region in (left) winter and (right) summer. Colors indicate depth of each particle (m). Particles located outside of the model domain after 30 days of backward tracking are not plotted. Solid black and dashed black contours depict 100 and 200 m isobaths, respectively. Cross-hatch area denotes the final position of the particles, i.e., the upwelling region.

are not considered. This does not significantly change the mean pathways of particles when large ensembles of trajectories are used to compute the Lagrangian pathways (Mason et al., 2012).

Each particle is backward tracked for a maximum of 45 days. Figure 9 illustrates the positions of particles 30 days before arriving at their final positions, in winter and summer. However, most particles have left the domain after backward tracking for 45 days, particularly in winter. The Scotian Current carries a high percent of the particles into the domain from the eastern direction. Hence, the variability of this current has a great impact on the transport rate of the particles. Figure 10 shows the mean pathway of particles for the 45 day backward tracking in winter and summer. In each season, two mean pathways are computed for particles originating from the eastern and western directions, separately.

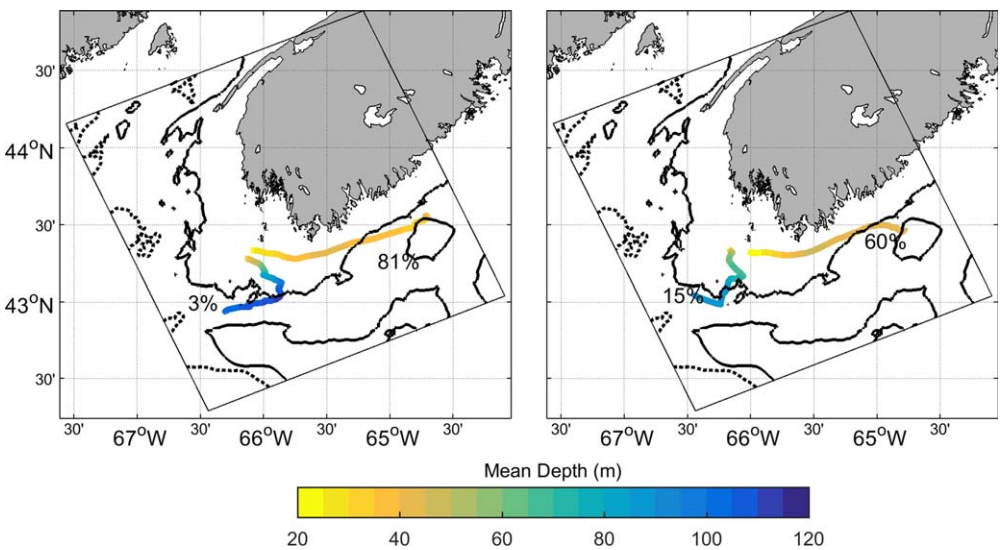

Figure 10. Same as Figure 9 but for the mean paths of particles 45 days before arriving at the final positions in the upwelling region in (left) winter and (right) summer. The particles are separated into groups, according to their physical originating positions from the eastern and western boundaries. The percentage of particles contributing to each mean path is indicated by numbers adjacent to the paths.

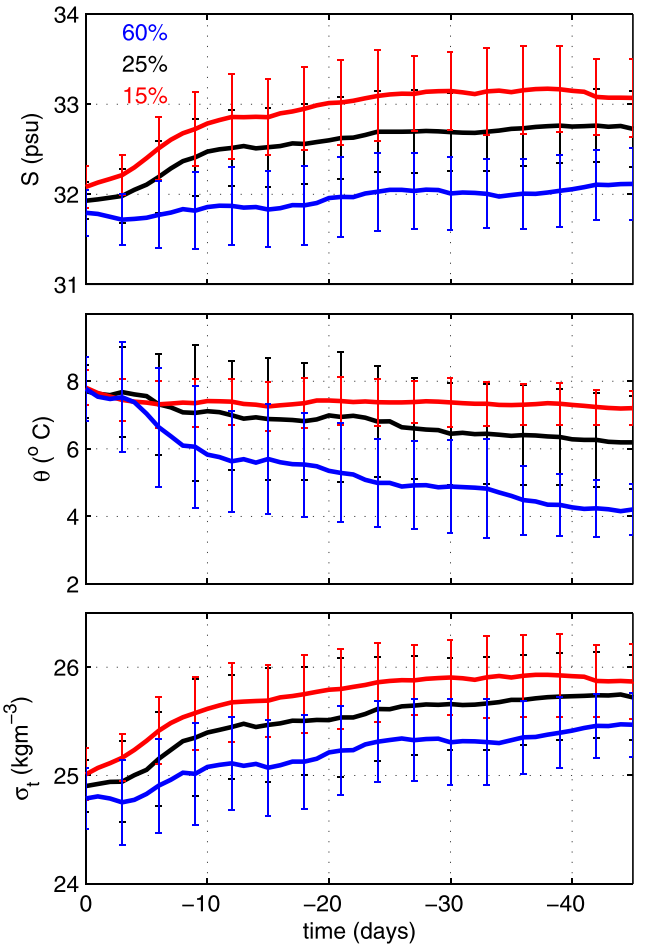

Figure 11. Summer mean and standard deviation of (top to bottom) salinity, temperature, and density along the paths of particles in time. Zero time value corresponds to when particles arrive at their final position in August. The along-path means are shown separately for particles entering from the eastern (blue) and western (red) boundaries or originate within the domain (black). The numbers in the top plot indicate the percentage of particles in each category. Vertical bars denote the standard deviations computed every 3 days.

In winter, 81% of the particles enter the domain from the eastern direction and most of these particles originate from the top 50 m depth. By contrast, only 3% of particles originate from the western direction mainly from deeper layers. In summer, possibly due to the weaker Scotian Current and strong mesoscale eddy activity, the physical original positions of particles are more scattered and particles from the eastern direction move slower to the upwelling region, compared with the situation in winter. In summer, 60% of the particles enter the domain from the eastern direction and 15% originate from the western direction.

The paths of the particles that originate from the eastern and western directions have different patterns. Entering from the eastern direction, the particles mainly follow the along-shore isobaths, taking about 20–45 days to arrive at the upwelling region. The mean path of these particles is closer to shore in summer than in winter, consistent with the seasonal variation of the Scotian Current position discussed in section 4. In both seasons, the majority of these particles originate from the surface layer with a mean depth of about 30 m. The particles with nearshore original positions (within 100 m isobaths) follow the along-shore branch of Scotian Current. Those originating from a more offshore region follow a longer path that goes around the small bank in the eastern part of the domain. About 5% of particles with an along-shore path undergo downwelling near 65°W longitude and upwell when arriving at the tidally mixed region (figures not shown).

Entering from the western direction, the particles move along offshore paths and cross isobaths to reach the upwelling region. The majority of these particles originate from latitudes south of 43°N, and follow the eastward current along the northern flank of the Browns Bank. The particles then move northward when reaching the region between 66°W and 65.5°W longitude, while crossing isobaths. Most of these particles originate from depths of 50 to 200 m, on average 110 and 130 m in summer and winter, respectively. The particles originating from the western direction take about 25–45 days to arrive at the upwelling region.

We now examine the original positions of particles with final positions above and below the summer mixed layer. Taking 25 m as the average depth of the summer mixed layer, 70% of particles originating from the eastern direction and 30% of particles originating from the western direction, have a final depth of less than 25 m. On average, particles originating from the eastern direction take 29 and 42 days to arrive at depths shallower and deeper than 25 m, respectively. The corresponding mean travel times are 40 and 44 days if coming from the western direction. The difference in travel time is related to difference in the paths of particles. For example, particles originating from the eastern direction take the shortest time to arrive above the upper mixed layer in the upwelling region because the paths of these particles follow closer to the shore.

Finally, we examine the variation of temperature, salinity, and density along the paths of particles in summer. For this calculation, at each time step of the particle tracking, the modeled temperature, salinity, and density are interpolated to the positions of particles under consideration by Arian. Figure 11 illustrates the variations of these properties for particles originating from eastern and western boundaries or remaining inside the domain after the 45 day backward tracking. Particles originating from the eastern boundary have the lowest along-path salinity, temperature, and density, corresponding to the properties of the Scotian Current. Particles entering from the western boundary correspond to the water mass properties of the Gulf of Maine and Northeast Channel region and have the highest temperature, salinity, and density. Particles originating from the western boundary show the largest salinity variation decreasing from 33 to 32 psu

when arriving at the upwelling region. Particles originating from the eastern boundary show the most significant path warming, increasing from 4°C to 8°C when reaching the upwelling region.

In addition to Lagrangian particle tracking using the Full run circulation, the effect of tidal forcing on upwelling is investigated by advecting particles using the BrtTide velocity fields. The particles are backward tracked for a maximum of 350 days because the magnitude of tidal residual currents is much smaller than the Full run currents. Results show that for particles originating outside the model domain to arrive in the upwelling region in less than 350 days, 54% and 46% of them enter from the western and eastern boundaries, respectively. The particles entering from both boundaries follow offshore paths advected by cross-isobath bottom currents. These particles mainly remain in the bottom layer and mix into the surface layer after arriving at the highly tidal mixing region. This evaluation indicates that in the Full run simulations, the motions of particles originating from the eastern direction are obstructed by nontidal flows. As discussed in section 4, the tidally onshore current is opposed by the offshore component of the Scotian Current preventing deeper layer particles from reaching the upwelling region. This is more evident in winter particle tracking simulations when the Scotian Current is stronger than in summer. Therefore, the Scotian Current variation plays an important role in modulating the tidally induced upwelling in the region.

6. Summary

A high-resolution baroclinic ocean model and Lagrangian particle tracking are used to study seasonal circulation and topographic upwelling off South West Nova Scotia. The SWNS model is forced with realistic meteorological forcing and downscaled from a larger model covering the Gulf of Maine and Scotian Shelf. Evaluation with observational data shows that this coastal model is able to simulate the seasonal circulation and hydrography and capture the well-known features of circulation in the region. The robustness of characterizing the seasonal variation off SWNS using 1 year model simulation is supported by multiyear observations of currents, temperature, and salinity analyzed in previous studies.

Model simulations are analyzed to quantify the main physical processes contributing to seasonal cross-shore and along-shore currents. It is shown that tidal forcing modifies the intensity of along-shore currents, opposing the westward Scotian Current and eastward inflow from the Northeast Channel. It is also confirmed that the near-bottom cross-isobath onshore currents are tidally induced. In summer, the onshore near-bottom currents are present over a large area in the region, including the whole subsurface layer near or inside the tidally mixed upwelling region. In winter, however, these currents are only present in deeper regions outside the tidal mixing area. The Scotian Current opposes the cross-isobath onshore currents, therefore its seasonal variability plays an important role on the topographic upwelling variability.

Lagrangian particle tracking is used to study the pathway of source waters arriving at the upwelling region off SWNS. Using the hourly velocity field of the Full run, two major groups of source waters are identified. In the first group, particles originating from the eastern direction are carried by the Scotian Current. Based on 45 day backward tracking, these particles constitute 81% and 60% of the total number of particles in winter and summer, respectively. These particles mainly originate from the top 50 m depth. In the second group, particles originate from the Gulf of Maine and the Northeast Channel and enter from the western direction. Based on 45 day backward tracking, these particles make up for 3% and 15% of the total number of particles in winter and summer, respectively. The western source particles originate from deeper layers with a mean depth exceeding 100 m. They travel in the near-bottom layer and cross isobaths before arriving at the upwelling region.

Particle tracking using BrtTide velocity fields shows that the percentage and pathway pattern of particles entering from the western and eastern boundaries are comparable. Both groups of particles follow tidally induced near-bottom onshore currents, crossing isobaths before reaching the tidal mixing (upwelling) region. This result is consistent with previous findings by Tee et al. (1993). The novel aspect of the present study is the significant role played by nontidal processes revealed by comparing the results of Full, NoTide, and BrtTide runs. In particular, the Full run solution shows that the Scotian Current opposes deeper layer particles from the eastern part of the domain to reach the upwelling region. Therefore, the Scotian Current variation plays an important role in modulating the tidally induced upwelling in the region.

Acknowledgments
We are very grateful to Professor Keith Thompson for his constant support and guidance throughout this study. We would like to thank Dr. Jean-Philippe Paquin for his help in setting up the numerical model and Dr. David Greenberg for many constructive and insightful comments. We also appreciate the provision of observational data by Dr. Peter C. Smith and Herman Varma. Two anonymous reviewers provided very constructive comments on the original manuscript. This work was supported by Marine Environmental Observation, Prediction, and Response (MEOPAR), funded by the Networks of Centres of Excellence of Canada Program. The observational data are available at http://www.bio.gc.ca/science/data-donnees/base/data-donnees/odi-eng.php. The NEMO and ARIANE codes can be obtained from https://www.nemo-ocean.eu and http://stockage.univ-brest.fr/~grima/Ariane/, respectively. The CGRF atmospheric forcing is available via http://goapp.ocean.dal.ca/index.php. The ARIANE and NEMO model run files for SWNS are available at http://doi.io-warnemuende.de/10.12754/data-2018-0001.

References

Amante, C., & Eakins, B. W. (2009). *ETOPO1 1 arc-minute global relief model: Procedures, data sources and analysis* (NOAA Tech. Memo. NESDIS NGDC-24, 19 pp.). Silver Spring, MD: National Oceanic and Atmospheric Administration.

Blanke, B., & Raynaud, S. (1997). Kinematics of the Pacific equatorial undercurrent: An Eulerian and Lagrangian approach from GCM results. *Journal of Physical Oceanography*, *27*, 1038–1053.

Chen, C., Beardsley, R., & Franks, P. J. (2001). A 3-D prognostic numerical model study of the Georges Bank ecosystem. Part I: Physical model. *Deep-Sea Research Part II*, *48*(1), 419–456.

Chen, C., Beardsley, R. C., & Limeburner, R. (1995). A numerical study of stratified tidal rectification over finite-amplitude banks. Part II: Georges Bank. *Journal of Physical Oceanography*, *25*(9), 2111–2128.

Chen, C., Huang, H., Beardsley, R. C., Xu, Q., Limeburner, R., Cowles, G. W., et al. (2011). Tidal dynamics in the Gulf of Maine and New England Shelf: An application of FVCOM. *Journal of Geophysical Research*, *116*, C12010. https://doi.org/10.1029/2011JC007054

Daley, R. (1993). *Atmospheric data analysis* (457 pp.). Cambridge, UK: Cambridge University Press.

Dever, M., Hebert, D., Greenan, B., Sheng, J., & Smith, P. (2016). Hydrography and coastal circulation along the Halifax line and the connections with the Gulf of St. Lawrence. *Atmosphere-Ocean*, *54*(3), 199–217.

Engedahl, H. (1995). Use of the flow relaxation scheme in a three-dimensional baroclinic ocean model with realistic topography. *Tellus, Series A*, *47*(3), 365–382.

Flather, R. A. (1994). A storm surge prediction model for the northern Bay of Bengal with application to the cyclone disaster in April 1991. *Journal of Physical Oceanography*, *24*(1), 172–190.

Fournier, R., Van Det, M., Hargreaves, N., Wilson, J., Clair, T., & Ernst, R. (1984). Physical factors controlling summer distribution of chlorophyll a off southwestern Nova Scotia. *Limnology and Oceanography*, *29*(3), 517–526.

Greenberg, D. A. (1979). A numerical model investigation of tidal phenomena in the Bay of Fundy and Gulf of Maine. *Marine Geodesy*, *2*(2), 161–187.

Hannah, C. G., Shore, J. A., Loder, J. W., & Naimie, C. E. (2001). Seasonal circulation on the western and central Scotian Shelf. *Journal of Physical Oceanography*, *31*(2), 591–615.

Katavouta, A., & Thompson, K. R. (2016). Downscaling ocean conditions with application to the Gulf of Maine, Scotian Shelf and adjacent deep ocean. *Ocean Modelling*, *104*, 54–72.

Katavouta, A., Thompson, K. R., Lu, Y., & Loder, J. W. (2016). Interaction between the tidal and seasonal variability of the Gulf of Maine and Scotian Shelf region. *Journal of Physical Oceanography*, *46*(11), 3279–3298.

Large, W. G., & Yeager, S. G. (2004). *Diurnal to decadal global forcing for ocean and sea-ice models: The data sets and flux climatologies* (NCAR Tech. Note NCAR/TN-460+STR, 111 pp.). Boulder, CO: CGD Division of the National Center for Atmospheric Research.

Lauzier, L. (1967). Bottom residual drift on the continental shelf area of the Canadian Atlantic coast. *Journal of the Fisheries Research Board of Canada*, *24*(9), 1845–1859.

Lee, S.-H., & Beardsley, R. C. (1999). Influence of stratification on residual tidal currents in the Yellow Sea. *Journal of Geophysical Research*, *104*(C7), 15679–15701.

Levier, B., Tréguier, A., Madec, G., & Garnier, V. (2007). *Free surface and variable volume in the NEMO code* (MERSEA IP Rep. WP09-CNRS-STR03-1A). France: Ifremer.

Lively, R. (1985). *Current meter, meteorological, and sea-level observations off Cape Sable, Nova Scotia, August 1980 to April 1983* (Canadian Data Report of Hydrography and Ocean Sciences, Vol. 40, 494 pp.). Canada: Department of Fisheries and Oceans.

Madec, G. (2008). *NEMO ocean engine* (Note du Pole de modélisation, No 27). Paris, France: IPSL. Retrieved from https://www.nemo-ocean.eu/bibliography/documentation/

Mason, E., Colas, F., & Pelegrí, J. L. (2012). A Lagrangian study tracing water parcel origins in the Canary upwelling system. *Scientia Marina*, *76*(S1), 79–94.

Ohashi, K., Sheng, J., Thompson, K. R., Hannah, C. G., & Ritchie, H. (2011). Effect of stratification on tidal circulation over the Scotian Shelf and Gulf of St. Lawrence: A numerical study using a three-dimensional shelf circulation model. *Ocean Dynamics*, *59*(6), 809–825.

Rivas, D., & Samelson, R. (2011). A numerical modeling study of the upwelling source waters along the Oregon coast during 2005. *Journal of Physical Oceanography*, *41*(1), 88–112.

Smagorinsky, J. (1963). General circulation experiments with the primitive equations: I. the basic experiment. *Monthly Weather Review*, *91*(3), 99–164.

Smith, G. C., Roy, F., Mann, P., Dupont, F., Brasnett, B., Lemieux, J.-F., et al. (2014). A new atmospheric dataset for forcing ice-ocean models: Evaluation of reforecasts using the Canadian global deterministic prediction system. *Quarterly Journal of the Royal Meteorological Society*, *140*(680), 881–894.

Smith, P. C. (1983). The mean and seasonal circulation off southwest Nova Scotia. *Journal of Physical Oceanography*, *13*(6), 1034–1054.

Smith, P. C. (1989). Seasonal and interannual variability of current, temperature and salinity off southwest Nova Scotia. *Canadian Journal of Fisheries and Aquatic Sciences*, *46*(S1), s4–s20.

Sutcliffe, W. Jr., Loucks, R., & Drinkwater, K. (1976). Coastal circulation and physical oceanography of the Scotian Shelf and the Gulf of Maine. *Journal of the Fisheries Research Board of Canada*, *33*(1), 98–115.

Tee, K. T. (1994). Dynamics of a two-dimensional topographic rectification process. *Journal of Physical Oceanography*, *24*(2), 443–465.

Tee, K.-T., Smith, P. C., & Lefaivre, D. (1988). Estimation and verification of tidally induced residual currents. *Journal of Physical Oceanography*, *18*(10), 1415–1434.

Tee, K. T., Smith, P. C., & Levaivre, D. (1993). Topographic upwelling off southwest Nova Scotia. *Journal of Physical Oceanography*, *23*(8), 1703–1726.

Umlauf, L., & Burchard, H. (2003). A generic length-scale equation for geophysical turbulence models. *Journal of Marine Research*, *61*(2), 235–265.